A Simplified Control Scheme for Electric Vehicle-Power Grid Circuit with DC Distribution and Battery Storage Systems

Kabeya Musasa[1], Musole Innocent Muheme[1], Nnamdi Ikechi Nwulu[1] and Mammo Muchie[2]
[1]*Dept. of Electrical and Electronic Engineering Science, University of Johannesburg, South Africa*
[2] *DST/NRF SARChI Professor, Tshwane University of Technology, South Africa*
corresponding author: innoc.musolem@gmail.com

***Abstract*— Direct current (DC) system is becoming the major trend for future internal power grid of electric vehicles (EVs). Since DC power grid system has a different nature to conventional alternating current (AC) grid system, appropriate design of the controller for EV- grid circuit is mandatory. In this paper, an EV employing a pure DC grid circuit with battery storage system (BSS) is considered as a study case. To enable a more efficient use of BSS, a flyback DC-DC converter for batteries charger/or discharger strategy is selected, which satisfy the power flows requirements. The dynamic and control performances of the combined system, i.e. "BSS- flyback DC-DC converter- connected to a DC motor", is investigated in terms of voltage/ current signal fluctuations. The small-signal based control method is used, which limits the small-signal variations to about zero. To verify the effectiveness of the control strategy several simulations are done using Matlab. The simulation results illustrate the performances obtained.**

***Index Terms*— batteries, control design, DC-DC power converters, electric vehicles, power grids.**

I. INTRODUCTION

The negative environmental impacts of the existing transportation system have made it mandatory to search for alternative solutions to prevent vast environmental pollution. The introduction of electric vehicles (EV) has proved that they are very much environmental friendly and emit fewer pollutants compared to vehicles with petrol/diesel engine (Sankara and Seyezhai 2016). Globally, the concept of electrical powered road vehicles is developing very fast. It has a good chance of becoming a significant part of the transportation infrastructure in the near future.

Among the components that are actually needed in an EV- power grid circuit include: an electric drive or electric motor, a power converter with controller scheme, a battery storage system (BSS), etc. Fig. 1 shows an exemple of an electric power grid scheme for an EV (Biradar, Patil and Ullegaddi 1998). The energy that flow into the EV-power grid comes directly from the BSS. In (Sankara and Seyezhai 2016) and (Biradar, Patil and Ullegaddi 1998), the BSS was combined with the photovoltaic (PV) solar system to power up the EV-power grid. The operating principle of a PV solar for EV can be found in (Sankara and Seyezhai 2016).

They are three different types of EV models that are actually being developed for use in the transportation sector to reduce the environment pollution problem, these include: the hybrid electric vehicles (HEVs), the plug-in hybrid electric vehicles (PHEVs), and the pure battery electric vehicles (BEVs) (Young et al. 2013) (Momoh and Omoigui 2009). The HEVs have gained a lot of popularity nowadays. But pure BEVs are the top highly developed models.

This paper analyses the control circuit of a pure BEV model. The BSS is the fundamental component of BEV; this power ups the EV-electric motor through a power electronic converter. The batteries for EVs are different from those used in small electronic devices like laptops and cell phones. The batteries for EV require handling high power or high energy capacity and also they must be very compact or small in size and weight for them to be installed within a limited space. Extensive research works are actually being given much attention to develop advanced battery technologies that are suitable for EVs all over the world (Young et al. 2013).

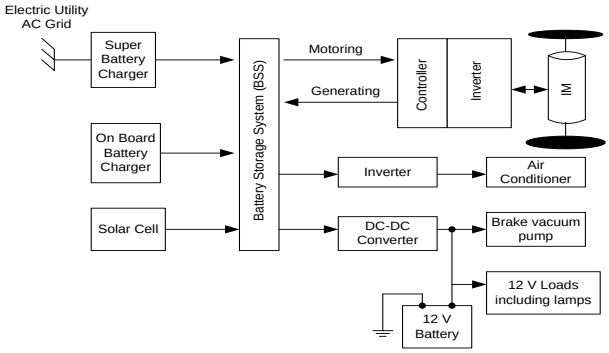

Figure 1. Sample of a power grid scheme for an EV (Biradar, Patil and Ullegaddi 1998)

Furthermore, in order to enable a more efficient use of energy from BSS, a dedicated power electronic converter for batteries charger/or discharger strategy must be selected, which can satisfy the power flow requirements. In this paper an isolated flyback DC-DC converter is selected to interface the BSS to a DC motor. In (Anwar et al. 2016), the dual active bridge (DAB) DC-DC converter was used to interface the BSS to a DC motor. The DAB DC-DC converter consists of a high-frequency inverter, a high-frequency transformer, and a high-frequency active bridge-rectifier. This converter topology enables a bidirectional power flow between the BSS and the DC motor.

The bidirectional operating condition of the power converter is necessary in EV–power grid circuits; because, in the armature winding of the DC motor, a back- electromagnetic force (emf) is generally produced by the rotation of armature conductors in the presence of field (or flux). The energy extracted from the back-emf can be useful to recharge the BSS. But such scheme will require a very complex EV- power grid circuit.

Instead of using the DAB DC-DC converter topology to interface the BSS and the DC motor, a single active bridge (SAB) DC-DC converter topology can also be used. The SAB DC-DC converter topology consists of a high-frequency inverter, a high-frequency transformer, and a high-frequency diode bridge-rectifier. Actually, the SAB DC-DC converter topology does not permit a bidirectional power flow between BSS and DC motor because of the passive diode-bridge rectifier. In (Pany, Singh and Tripathi 2011), the bidirectional DC-DC buck converter was selected to interface the BSS and the DC motor. A three-phase full-bridge DC-DC converter was considered in (Kumar and Gaur 2014). And the buck-boost DC-DC converter was used in (Albiol-Tendillo et al. 2012). In all these papers, the DC-DC converters were properly selected, but, there was no specific control strategy elaborated.

The types of electric drives or motors used for EVs includes brushed DC motor, brushless DC motor, AC induction motor, permanent magnet synchronous motor (PMSM) and switched reluctance motor (SRM) (Huang, Li and Chen 2010). The fact that the power output of BSS is DC power, DC motor is selected in this paper to drive the EV wheels. There are three types of brushed DC motor with field windings, which are the series, shunt and separately excited windings (Huang, Li and Chen 2010). Topology of DC motors for EV with magnet ring and stator winding are also presented in (Lovatt, Ramsden and Mecrow 1998).

In this paper, the dynamic and control strategy of the combined system, i.e. “BSS- flyback DC-DC converter-connected to a DC motor”, is investigated in terms of voltage/current signal fluctuations. The dynamic model of the flyback DC-DC converter is also derived. The small-signal based control method is used, which limits the small-signal variations to about zero. The effectiveness of the control strategy which is provided by the flyback DC-DC converter is tested by using an arbitrary EV-data. To verify the effectiveness of the control strategy several simulations are done using Matlab.

II. EV-POWER GRID: SIMPLIFIED EQUIVALENT BLOCK DIAGRAM

Fig. 2a presents a simplified equivalent block diagram of the EV- power grid to be discussed in this paper. The EV-power grid includes a control scheme installed across the flyback DC-DC converter, depicted by Fig. 2b, and an electric DC motor connected to two wheels via a transmission box. The DC motor is powered by a BSS via a flyback DC-DC converter. The batteries can be interconnected either in series to increase the voltage or in series-parallel to increase both the voltage and the current or power. The batteries are recharged from the mains electrical network.

Typical EV-power grid circuit with a single closed-loop control scheme was discussed in (Santos et al. 2007). The flyback DC-DC converter controls the power delivered to the DC motor through variation of the converter switches duty ratio. Based on Fig. 2b, the gate drive circuit, which consists of a pulse-width modulation (PWM) scheme, commands the state of the switches of the flyback DC-DC converter. Depending on the performance to achieve, the current controller or compensator in the current-loop system can either be the proportional-integral (PI) or the proportional–integral–derivative (PID) controller. A filter can also be required at the output of the DC-DC converter to reduce the ripple current in the DC motor.

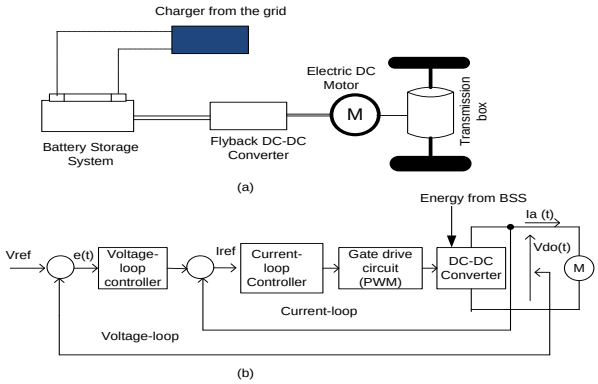

Figure 2. Simplified equivalent block diagram of an EV. (a) Power grid circuit; (b) control scheme installed across the flyback DC-DC converter.

II.1. DC motor: principle of operation

In a DC motor, the field flux ϕ_f is established by the stator, either by means of permanent magnets, where ϕ_f = constant, or by means of a field winding, where ϕ_f is controlled by i_f; as given by eq. (1) (Mohan, Undeland and Robbins 2003), with k_f being the field constant of proportionality, and $i_f(t)$ the field current.

$$\phi_f = k_f i_f \tag{1}$$

The armature winding on the rotor side carries out the electrical power from BSS via the split-ring commutator/ or brushes. The electromagnetic torque is produced by the interaction of $\phi_f(t)$ and $i_a(t)$, as eq. (2) (Pany, Singh and Tripathi 2011), where $i_a(t)$ is the armature winding current, and k_t the torque constant of the rotor.

$$T_{em} = k_t \phi_f i_a \tag{2}$$

The armature current $i_a(t)$ is determined by a controllable $v_{do}(t)$ (i.e. the output voltage of the flyback DC-DC converter), by the armature winding resistance r_a, by the armature winding inductance L_a, and by the induced back-emf $e_a(t)$; this is derived in Laplace domain as eq. (3).

$$i_a(s) = \frac{v_{do}(s) - e_a(s)}{r_a + L_a s} \tag{3}$$

The back-emf is produced by the rotation of armature conductors at speed ω_m in the presence of $\phi_f(t)$, as eq. (4) (Veilleux and Lehn 2014), where k_e is the voltage constant of the electric motor.

$$e_a(t) = k_e \phi_f \omega_m \tag{4}$$

Based on Fig. 2a, the DC motor is driving two wheels through a transmission box at a speed of ω_m. During the braking operation: if $|v_{do}(t)| < |e_a(t)|$, $|i_a(t)|$ will reverse in direction, also T_{em} defined by eq. (2) will reverse in direction. As a result, the kinetic energy associated with the motor inertia is converted into electrical energy by the DC machine, which acts as a DC generator. This energy can either be dissipated in a resistor or absorbed by BSS. As ω_m decreases (the motor slows down) and $e_a(t)$ decreases in magnitude.

A. DC motor with magnet ring

The permanent magnets on the stator side produce a constant ϕ_f, and thus eq. (2), (3), and (4) will not depend on the field current i_f. As a result, eq. (2), (3), and (4) can, respectively, take the form in eq. (5) :

$$T_{em} = k_T i_a \text{ ; } V_{do} = E_a + r_a i_a \text{ ; and } e_a(t) = k_{PM} \omega_m \tag{5}$$

where $k_T = k_t \phi_f$ and $k_{PM} = k_e \phi_f$. From eq. (5), one can derive the expression of ω_m in terms of T_{em} given different values of $v_{do}(t)$: i.e. the torque-speed characteristics, eq. (6):

$$\omega_m = \frac{1}{k_{PM}} \left(v_{do}(t) - \frac{r_a}{k_T} T_{em} \right) \tag{6}$$

Based on eq. (6), it is noted that the rotating speed of wheels for an EV with permanent magnet DC motor is controlled by controlling the output voltage of the flyback DC-DC converter, $v_{do}(t)$.

B. DC motor with separately excited winding

Permanent magnet based DC motors have maximum speed limitation. To overcome this limitation, the field winding on the stator side is excited by a separately controlled DC source. Using eq. (1), $\phi_f(t)$ is controlled through $i_f(t)$, and thus eq. (6) can take the form in eq. (7).

$$\omega_m = \frac{1}{k_e \phi_f} \left(v_{do}(t) - \frac{r_a}{k_t \phi_f} T_{em} \right) \tag{7}$$

From eq. (7), it is noted that the rotating speed of wheels in an EV employing DC motor with separately excited winding, is controlled by controlling both the output voltage of the flyback DC-DC converter $v_{do}(t)$ and the field winding $\phi_f(t)$.

II.2. Effect of armature voltage and current ripples

Based on Fig. 2, the output voltage of the flyback DC-DC converter may contains small signal variations, which can lead further to a ripple in the armature current. This will result into a high form factor, high losses in the DC motor, and hence, low efficiency of the DC motor. The form factor is defined as the ratio between the armature current (rms) and the armature current (average). If i_a is a pure DC signal, then the form factor is unit. The form factor increase when the signal i_a contains small variations or deviate from a pure DC signal.

In addition, from eq. (2), $T_{em}(t)$ depends of $i_a(t)$; thus, a ripple in $i_a(t)$ will result in the torque pulsation, which will lead further to a ripple in ω_m.

III. EV SERVO DRIVE: EQUIVALENT MODEL

The proposed EV-controller scheme or -regulator block diagram to compensate the voltage/current ripple is depicted by Fig. 3a (Musasa, Gitau and Bansal 2015a, Musasa, Gitau and Bansal 2015b); the different transfer functions or equivalent model of the flyback DC-DC converter are derived further in eq. (8), (9), and (10).

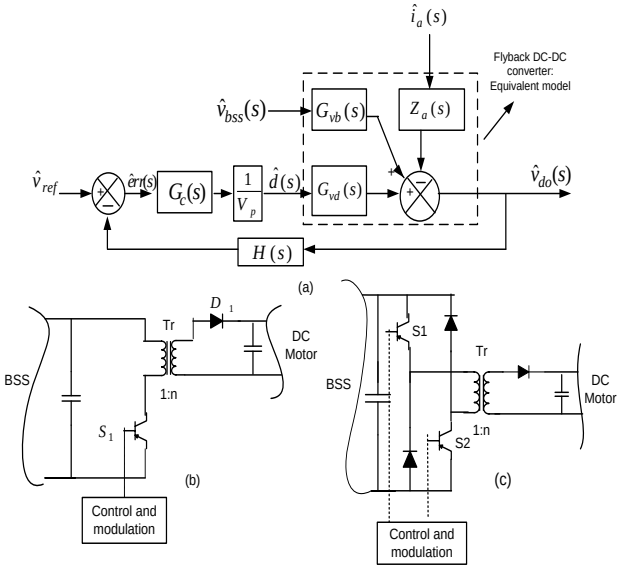

Figure 3. (a) Block diagram of the control scheme. It enables compensating the small current/voltage signal variations; (b) the single active-switch flyback DC-DC converter; and (c) the double active-switch flyback DC-DC converter, this is an alternative topology of the single-switch flyback converter which limits the voltage spike.

The inputs to the regulator are the voltage and current ripples. These ripples are originating from the BSS or the DC motor, or any other phenomena. The symbol (^) stand for small signal variations or ripple. The topology of the isolated flyback DC-DC converter is shown in Fig. 3b. The goal of this converter is to regulate and smooth the net power injected to the DC motor. Only a single active switch is installed in this converter topology; the overvoltage spike is applied frequently across the single switch S_1 at each turn off. The peak value of this overvoltage depends upon the switching time.

In practice, the single- active- switch flyback DC-DC converter requires a snubber circuit to limit the voltage spike across the switch S_1. The double-active-switch flyback DC-DC converter, depicted by Fig. 3c, is another option that can be considered to limit the voltage spike across switch S_1.

II.1. Flyback DC-DC converter: equivalent models

On Fig. 3b, the flyback transformer has an equivalent magnetizing inductance L_{eq}, and turn ratio 1: n; switch S_1 has on-resistance R_{on}; $err(t)$ is the steady-state error; the transformer leakage inductances and the switching loss are negligible.

The transfer functions in Fig. 3a are derived in eq. (8), (9), and (10); the derivation method of these transfer functions can be found in (Musasa, Gitau and Bansal 2015b, Erickosn 2001), where $G_{vb}(s)$ represents the effect of BSS-output voltage variations on $v_{do}(s)$; $G_{vd}(s)$ represents the effects of duty ratio variations on $v_{do}(s)$; $Z_a(s)$ represents the effects of armature current variations on $v_{do}(s)$; V_{do} and V_{bss} are, respectively, the steady-state voltage input to the DC motor and output terminal of the BSS.

$$G_{vb}(s)=\frac{\hat{v}_{do}}{\hat{v}_{bss}}=\left(-\frac{Dn}{1-D}\right)\frac{1}{1+s\left(\frac{L_{eq}n^2}{(1-D)^2 r_a}\right)+s^2\left(\frac{L_{eq}Cn^2}{(1-D)^2}\right)} \tag{8}$$

$$G_{vd}(s)=\frac{\hat{v}_{do}}{\hat{d}(s)}=\left(\frac{V_{do}-V_{bss}}{1-D}\right)\frac{1-s\left(\frac{L_{eq}I_a}{(1-D)(V_{bss}-V_{do})}\right)}{1+s\left(\frac{L_{eq}n^2}{(1-D)^2 r_a}\right)+s^2\left(\frac{L_{eq}Cn^2}{(1-D)^2}\right)} \tag{9}$$

$$Z_a(s)=\frac{\hat{v}_{do}}{\hat{i}_a}=\frac{s\frac{L_{eq}n^2}{(1-D)^2}}{1+s\frac{L_{eq}n^2}{r_a(1-D)^2}+s^2\frac{L_{eq}Cn^2}{(1-D)^2}} \tag{10}$$

The regulator system, Fig. 3a, is designed in order to adjust automatically the duty cycle as necessary to obtain a desired $v_{do}(s)$ regardless of disturbances in EV-power grid circuit parameters.

The inductor and capacitor of the flyback DC-DC converter can be sized using equation (11) and (12), respectively, where Δi_{pk-pk} and Δv_{pk-pk} are respectively specified peak-to-peak inductor current and capacitor voltage ripples. The steady-state component of the duty cycle can be determined using equation (13). However, these values can be adjusted such that a given or desired performance is achieved.

$$L_{eq}=\frac{V_{bss}-I_{pcc}R_{on}}{\Delta i_{pk-pk}}DT_s \tag{11}$$

$$C=\frac{V_{pcc}DT_s}{R_{pcc}\Delta v_{pk-pk}} \tag{12}$$

$$D\approx\frac{V_{do}}{V_{do}+V_{bss}} \tag{13}$$

III.2. Design of compensator transfer function

It is desired to achieve a constant voltage $v_{do}(t)=V_{do}$, in spite of disturbances in EV-parameters. Technically, it may be impossible to achieve such a condition without the use of a compensator in the feedback control-loop system. The compensator or controller $G_c(s)$ is generally designed to attain adequate phase margin and good rejection of expected disturbances, or to reduce the influence of $\hat{v}_{do}(t)$ on the armature current $i_a(t)$.

The Proportional Integral Derivative (PID) compensator or the combined lead-lag compensator system can lead to a very small steady-state error and better rejection of disturbances. Based on the regulator block diagram of Fig. 3a, the closed-loop transfer functions are derived in eq. (14), (15), and (16), where $T_v(s)$ is the voltage loop gain given by equation (17); $H(s)$ is the voltage sensor gain; and V_P is the peak magnitude of the PWM triangular signal.

$$G_{v\_vref}(s)=\frac{\hat{v}_{do}(s)}{\hat{v}_{ref}(s)}=\frac{1}{H(s)}\frac{T_v(s)}{1+T_v(s)} \tag{14}$$

$$G_{v\_vbss}(s)=\frac{\hat{v}_{do}(s)}{\hat{v}_{bss}(s)}=\frac{G_{vb}(s)}{1+T_v(s)} \tag{15}$$

$$G_{v\_i}(s) = \frac{\hat{v}_{do}(s)}{\hat{i}_a(s)} = -\frac{Z_{pcc}(s)}{1+T_v(s)} \tag{16}$$

$$T_v(s) = H(s)G_c(s)G_{vd}(s)/V_P \tag{17}$$

The feedback control-loop system of Fig. 3a is stable when the phase margin of $T_v(s)$ is positive; the phase margin is defined by eq. (18), where f_c is the crossover frequency.

$$\varphi_m = 180^\circ + \angle T_v(j2\pi f_c) \tag{18}$$

Thus to ensure a stable feedback loop system the characteristic in eq. (19) must be achieved:

$$\angle T_v(j2\pi f_c) > -180^\circ \tag{19}$$

In addition, φ_m must be sufficiently large to limit the amount of overshoot and ringing; also, $T_v(s)$ must be sufficiently large in magnitude to limit the magnitude of $Z_a(s)$ and $G_{vb}(s)$ based on eq. (15) and (16). Furthermore, the transient response time can be shortened by increasing the feedback loop crossover frequency. All these specifications can be achieved by a proper design of $G_c(s)$ in eq. (17).

The PID compensator has a transfer function given by equation (20) (Erickosn 2001),

$$G_c(s) = K_c \frac{\left(1+\frac{2\pi f_L}{s}\right)\left(1+\frac{s}{2\pi f_z}\right)}{\left(1+\frac{s}{2\pi f_{p1}}\right)\left(1+\frac{s}{2\pi f_{p2}}\right)} \tag{20}$$

where f_L is the inverted zero which improves the low-frequency regulation; K_c is the constant gain of $G_c(s)$; f_z is the zero frequency which adds a phase lead at the vicinity of the crossover frequency; and f_{p1} and f_{p2} are the high-frequency poles which prevent the switching ripple from disrupting the operation of the PWM.

IV. PID CONTROLLER: PERFORMANCE ANALYSIS

Based on Fig. 3, let's consider a BSS with a nominal output voltage $v_{bss} \approx V_{bss}$ = 40 V DC ($\hat{v}_{bss} \approx 0$). It is desired to maintain a regulated voltage V_{do} = 100 V DC at the input of the DC motor. By assuming a small armature resistance, $r_a = 2\ \Omega$; the steady-state armature current is obtained as $I_a = 50$ A. A voltage reference of 5 V is selected, and thus $H(s) = V_{ref}/v_{do} = 0.05$ ($err(s) \approx 0$). The steady-state value of the duty cycle is obtained using eq. (13), $D \approx 0.7$; the switching frequency is given $f_s = 1/T_s = 3.5$ kHz. The network components of the flyback converter can be sized using eq. (11) and (12) or can be selected from the "market list of available components": (assuming that: $L_{eq}n^2 \approx 1\ H$ and $Cn^2 \approx 0.5\ F$). The voltage loop gain $T_v(s)$ is therefore obtained by substitution of eq. (9) and (20) into (17).

The characteristic of the uncompensated voltage loop gain $T_u(s)$, with unity compensator gain $G_c(s) = 1$, is sketched in Fig. 4. It can be seen that the uncompensated loop gain has a very small crossover frequency of approximately 0.25 Hz, with a small phase margin of less than 10 degrees. With this control performance, larges transient response time and high overshoot and ringing will be expected in $v_{do}(t)$ for a step change in EV- parameters.

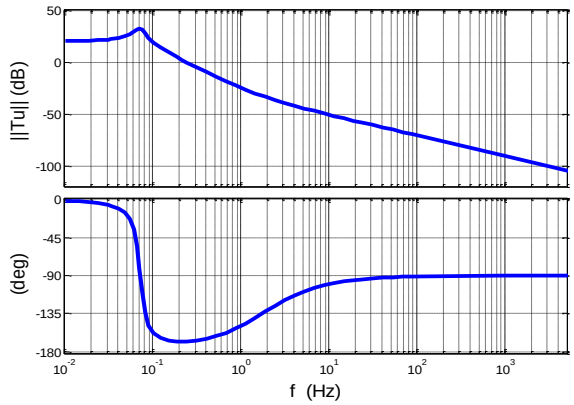

Figure 4. Characteristic of the uncompensated loop gain with $G_c(s) = 1$

Let now include a compensator system eq. (20) into eq. (17) to achieve a sufficiently large crossover frequency and phase margin. For example, let achieve a crossover frequency of a least one tenth of the switching frequency and a phase margin higher than 60 degrees. The zero and poles frequencies in eq. (20) can be obtained using eq. (21) and (22). The constant gain is obtained using equation (23), where T_{u0} is the low-frequency magnitude of the uncompensated loop gain; f_L in equation (20) can be chosen arbitrarily, for example f_L = one-tenth of the crossover frequency or 35 Hz; and $f_0 = 1/2\pi(\sqrt{L_{eq}C})$.

$$f_z = (0.35kHz)\sqrt{\frac{1-\sin(60^\circ)}{1+\sin(60^\circ)}} \approx 0.1kHz \tag{21}$$

$$f_p = (0.35kHz)\sqrt{\frac{1+\sin(60^\circ)}{1-\sin(60^\circ)}} = 1.3kHz \tag{22}$$

$$K_c = \left(\frac{f_c}{f_0}\right)^2 \frac{1}{T_{u0}}\sqrt{\frac{f_z}{f_{p1,2}}} \tag{23}$$

The characteristic of the compensated loop gain is sketched in Fig. 5. It can be seen that the phase margin is larger than 60 degrees over the frequency range from 100Hz to high-frequency. The crossover frequency is moved from 0.25 Hz (in Fig. 4) to 0.35 kHz or 350 Hz in Fig. 5, thus the transient response time is shortened. Hence variations in i_a should have little impact on the phase margin. Also, the low-frequency voltage loop-gain magnitude has increased, from about 20 dB in Fig. 4 to 100 dB in Fig. 5, thus reduces effectively the magnitude of $Z_a(s)$ and $G_{vb}(s)$ in eq. (15) and (16).

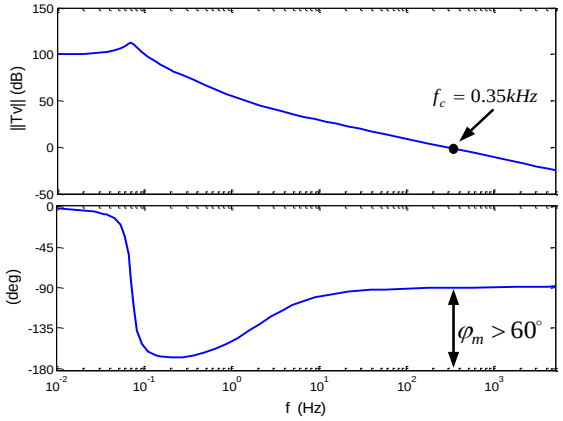

Figure 5. Characteristic of the compensated loop gain $T_v(s)$ with $G_c(s)$ = eq. (20).

V. CONTROL SYSTEM PERFORMANCE EVALUATION

Step changes or disturbances of magnitude $\| \hat{v}_{do} \|$ and $\| \hat{i}_a \|$ are respectively applied to the proposed scheme Fig. 3. The characteristics shown in Fig. 6 and 7 are obtained, respectively, for the system with no compensator ($G_c(s) = 1$) and for the system with a compensator ($G_c(s)$ = eq. (20)).

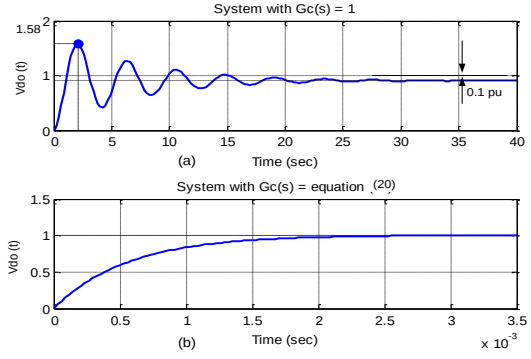

Figure 6. Characteristics of the voltage signal at the input of the DC motor when small variations of parameters (current, voltage, duty ratio) occur in the EV-power grid, (a) system with no compensator showing high overshoot, ringing, and steady-state error (b) system with a compensator showing no overshoot, ringing, and zero steady-state error.

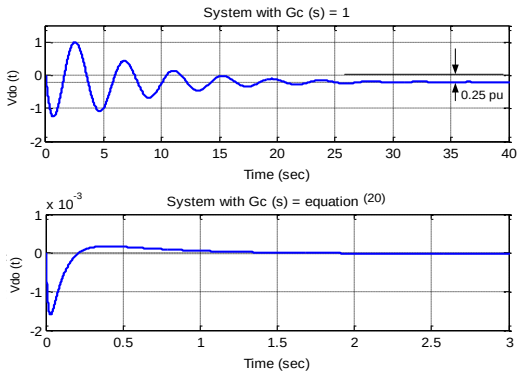

Figure 7. Characteristics of the voltage signal at the input of the DC motor when a step change occur in BSS output voltage, (a) system with no compensator showing high overshoot, ringing, and steady-state error (b) system with a compensator showing no overshoot, ringing, and zero steady-state error

It can be seen from Fig. 6b and 7b that the proposed controller scheme, which includes the compensator or controller $G_c(s) =$ eq. (20) in the closed-loop, maintains well the voltage variations at the input of the DC motor with zero steady-state error, no overshoot and ringing, in spite of step changes in EV- power grid parameters.

VI. CONCLUSION

The evaluated EV-power grid scheme, consisting of: "a BSS, an isolated flyback DC-DC converter with a controller, and a DC motor" performs well in maintaining the input voltage of the DC motor within acceptable limits of variation in spite of the variations of parameters in the EV-circuits and the effect of BSS charging/ discharging process. No overshoot and ringing are observed in the DC voltage characteristics; also, the steady-state error is kept to about zero. Further analyses can be conducted using PSim or PSCAD to investigate others performance such the fault ride through capability.

VII. REFERENCES

[1] Albiol-Tendillo L., Vidal-Idiarte E., Maixé-Altés J., Bosque-Moncusí J.M., and Valderrama-Blavi H. 2012. "Design and Control of a Bidirectional DC/DC Converter for an Electric Vehicle." Paper presented at the 15th International Power Electronics and Motion Control Conference (EPE/PEMC), Novi Sad, Serbia, 4-6 Sept. 2012.

[2] Anwar S., Zhang W., Wang F. and Costinett D. J. 2016. "Integrated DC-DC Converter Design for Electric Vehicle Power trains." Paper presented at the IEEE Applied Power Electronics Conference and Exposition (APEC),Long Beach, USA. 20-24 March 2016.

[3] Biradar S. K., Patil R. A., and Ullegaddi M. 1998. "Energy Storage System in Electric Vehicle." Paper presented at the Power Quality Conference, Hyderabad, India, 18 June 1998.

[4] Erickson R. W. 2001. *Fundamentals of Power Electronics*. Springer Publishers.

[5] Huang Q., Li J. and Chen Y. 2010. *Control of Electric Vehicle, Urban Transport and Hybrid Vehicles*. Intech Open Science Publishers.

[6] Kumar A. and Gaur P. 2014. "Bidirectional DC/DC Converter for Hybrid Electric Vehicle." Paper presented at the International Conference on Advances in Computing, Communications and Informatics (ICACCI), 24-27 Sept. 2014.

[7] Lovatt H.C., Ramsden V. S. and Mecrow B.C. 1998. "Design of an in Wheel Motor for Solar- Powered Electric Vehicles." *IEE Proceedings - Electric Power Applications* 145(5): 402-408.

[8] Mohan N., Undeland T.M., and Robbins W.P. 2003. *Power electronics: converters, applications, and design*. John Wiley & Sons, Inc.

[9] Momoh O. D. and Omoigui M. L. 2009. "An Overview of Hybrid Electric Vehicle Technology." Paper presented at the 5th IEEE Vehicle Power and Propulsion Conference, Dearborn, Michigan September 7-11, 2009.

[10] Musasa K., Gitau M.N., and Bansal R.C. 2015. "Performance analysis of power converter based active rectifier for an offshore wind park." *Electric Power Component and Systems* 43(8–10): 1089–1099.

[11] Musasa K., Gitau M.N., and Bansal R.C. 2015. "Dynamic analysis of DC–DC converter internal to an offshore wind farm', *IET Renewable Power Generation* 9(6): 542–548.

[12] Pany P., Singh R. K., and Tripathi R.K. 2011. "Bidirectional DC-DC converter fed drive for electric vehicle system." *International Journal of Engineering, Science and Technology* 3(3): 101-110.

[13] Sankara A.B. and Seyezhai R. 2016. "Simulation and Implementation of Solar Powered Electric Vehicle." *Circuits and Systems* 7: 643-661.

[14] Santos R., Pais F., Ferreira C., Ribeiro H., and Matos P. 2007. "Electric Vehicle- Design and Implementation Strategies for the Power Train." *Renewable Energy & Power Quality Journal* 1(5): 552-558.

[15] Veilleux E. and P.W. Lehn. 2014. “Interconnection of direct-drive wind turbines using a series-connected DC grid.” *IEEE Transaction on Sustainable Energy* **5**(1): 139–147.
[16] Young K., Wang C., Wang L. Y. and Strunz K. 2013. “Electric Vehicle Battery Technologies.” In Electric Vehicle Integration into Modern Power Networks, edited by Garcia-Valle R. and Pec¸as Lopes J.A. 15-56. Springer Publishers.